ADVANCED FUNCTIONAL MATERIALS
www.afm-journal.de

Hybrid Improper Ferroelectricity in Multiferroic Superlattices: Finite-Temperature Properties and Electric-Field-Driven Switching of Polarization and Magnetization

Bin Xu, Dawei Wang, Hong Jian Zhao, Jorge Íñiguez, Xiang Ming Chen, and Laurent Bellaiche**

The so-called hybrid improper ferroelectricity (HIF) mechanism allows to create an electrical polarization by assembling two nonpolar materials within a superlattice. It may also lead to the control of the magnetization by an electric field when these two nonpolar materials are magnetic in nature, which is promising for the design of novel magneto-electric devices. However, several issues of fundamental and technological importance are presently unknown in these hybrid improper ferroelectrics. Examples include the behaviors of its polarization and dielectric response with temperature, and the paths to switch both the polarization and magnetization under electric fields. Here, an effective Hamiltonian scheme is used to study the multiferroic properties of the model superlattice $(BiFeO_3)_1/(NdFeO_3)_1$. Along with the development of a novel Landau-type potential, this approach allows to answer and understand all the aforementioned issues at both microscopic and macroscopic levels. In particular, the polarization and dielectric response are both found to adopt temperature dependences, close to the phase transition, that agree with the behavior expected for first-order improper ferroelectrics. And most importantly, a five-state path resulting in the switching of polarization and magnetization under an electric field, via the reversal of antiphase octahedral tiltings, is also identified.

1. Introduction

The quest for room-temperature multiferroics, ideally for the low-power applications that utilize the electric field control of magnetization, remains very attractive after intensive efforts in the past decade.[1–3] Unfortunately, in typical ferroelectric (FE) oxides such as $BaTiO_3$, the spontaneous electric polarization is not compatible with magnetism, due to the empty 3*d* orbitals of the transition metal cation. Only a handful of multiferroics are known, but most of them are not suitable for practical applications, either because the polarization or magnetization is small (or only exist at low temperature) or because their mutual coupling is too weak.

Interestingly, a specific class of materials—the so-called hybrid improper ferroelectrics (HIF)—holds great promise toward the realization of room-temperature multiferroics.[4] Of special interest are superlattices (SLs) combining two perovskites that (1) both present antiferroelectric (AFE) displacements and (2) are stacked alternately as $(ABO_3)_1/(A'BO_3)_1$.[5,6] In these HIF systems, the spontaneous polarization is induced by another type of structural distortions, namely oxygen octahedral tiltings, which are also known to couple strongly with the magnetization, therefore providing an indirect coupling between polarization and magnetism.[5–8]

Several works based on density functional calculations have been devoted to better understand and characterize HIF,[5–9] and an atomistic theory has been developed to clarify its microscopic energetic origin.[10,11] Nevertheless, all these previous theoretical and computational studies are limited to 0 K properties,[5–9] and the finite-temperature behavior of HIF materials remains largely uninvestigated. For instance, one may wonder how the polarization and dielectric response evolve with temperature, whether it is similar to other types of ferroelectrics (e.g., proper,[12] improper,[13] or triggered-type[14,15]) or not. Moreover, while they are crucial to the great expectations that HIF is creating, the switching mechanisms of the polarization and magnetization under electric fields remain an open question.

Here, taking the $(BiFeO_3)_1/(NdFeO_3)_1$ SL as a representative and relevant example of the most interesting HIF materials,

Dr. B. Xu, Prof. L. Bellaiche
Physics Department and Institute for Nanoscience and Engineering
University of Arkansas
Fayetteville, Arkansas 72701, USA
E-mail: binxu@uark.edu; laurent@uark.edu
Dr. D. Wang
Electronic Materials Research Laboratory-Key Laboratory of the Ministry of Education and International Center for Dielectric Research
Xi'an Jiaotong University
Xi'an 710049, China
H. J. Zhao, Prof. X. M. Chen
Laboratory of Dielectric Materials
Department of Materials Science and Engineering
Zhejiang University
Hangzhou 310027, China
Dr. J. Íñiguez
Materials Research and Technology Department
Luxembourg Institute of Science and Technology (LIST)
5 avenue des Hauts-Fourneaux
L-4362 Esch/Alzette, Luxembourg, and Institut de Ciència de Materials de Barcelona (ICMAB-CSIC)
Campus UAB
08193 Bellaterra, Spain

DOI: 10.1002/adfm.201501113

we extensively investigate its finite-temperature and switching behaviors, using a numerical scheme we have recently developed.[16] We choose the $(BiFeO_3)_1/(NdFeO_3)_1$ SL, because (1) the *Pnma* phase, characterized by AFE distortions and $a^-a^-c^+$ oxygen octahedral tiltings in Glazer's notation,[17] is the ground state for $NdFeO_3$ (NFO)[18,19] and it is a metastable phase of $BiFeO_3$ (BFO) that is close in energy to the ground-state *R3c* phase;[20] (2) both BFO and NFO adopt a G-type AFM with high Néel temperatures (643 K for BFO[21] and 760 K for NFO;[22] and (3) weak ferromagnetism due to spin canting exists in both BFO[23–26] and NFO,[27,28] via a Dzyaloshiskii–Moriya (DM) interaction.[29,30] In the following, we first discuss the temperature dependence of various properties of $(BiFeO_3)_1/(NdFeO_3)_1$ superlattice, and compare them with those of $Bi_{0.5}Nd_{0.5}FeO_3$ disordered solid solution. In particular, it is found that both the polarization and dielectric response exhibit, close to the phase transition, temperature behaviors being identical to those of first-order improper ferroelectrics. A Landau-type formalism is then proposed, which reproduces well, and thus allows us to understand, such behaviors. Finally, we investigate the reaction of the SL to an applied electric field, and identify a five-state pathway that results in a deterministic switching of both the polarization and magnetization, thus attesting the promise of HIF materials for the design of future magnetoelectric devices. Strikingly, the observed switching mechanism relies on the presence and combination of three different trilinear energy couplings that we discuss in detail below.

2. Results and Discussion

2.1. AFE-Type Phases in $Bi_{0.5}Nd_{0.5}FeO_3$: Alloy Versus Superlattice

Here, we use the effective Hamiltonian numerical scheme recently developed in ref.[16] and detailed in the Experimental Section, in order to investigate finite-temperature behaviors of Nd-substituted BFO (BNFO) in both disordered and ordered forms. Disordered BNFO consists of a $(Bi_{0.5}Nd_{0.5})FeO_3$ solid solution in which Bi and Nd ions are randomly distributed within the A-sublattice of the ABO_3 perovskite structure. In contrast, ordered BNFO is constructed as the 1/1 superlattice with BFO/NFO layers alternating along the [001] pseudocubic direction (see the top left inset of Figure 2). As indicated in the Experimental Section, both systems are modeled by 16 × 16 × 16 supercells (thus containing 20 480 atoms), and the *x*-, *y*-, and *z*-axes are chosen to lie along the pseudocubic [100], [010], and [001] directions, respectively.

Figure 1a–c shows the temperature dependence of different structural and dielectric properties in the disordered solid solution. These properties are: (i) the supercell averages of the local modes (upper panel), with u_Γ and u_x characterizing the electrical polarization and AFE distortions associated with the *X*-point of the first Brillouin zone, respectively; (ii) the supercell averages of the axial vectors quantifying the oxygen octahedral tilting, with ω_R and ω_M corresponding to the rotations in antiphase and in-phase (also known as antiferrodistortive or AFD motions), respectively. Note that the directions of ω_R and ω_M indicate the axes about which the antiphase and in-phase

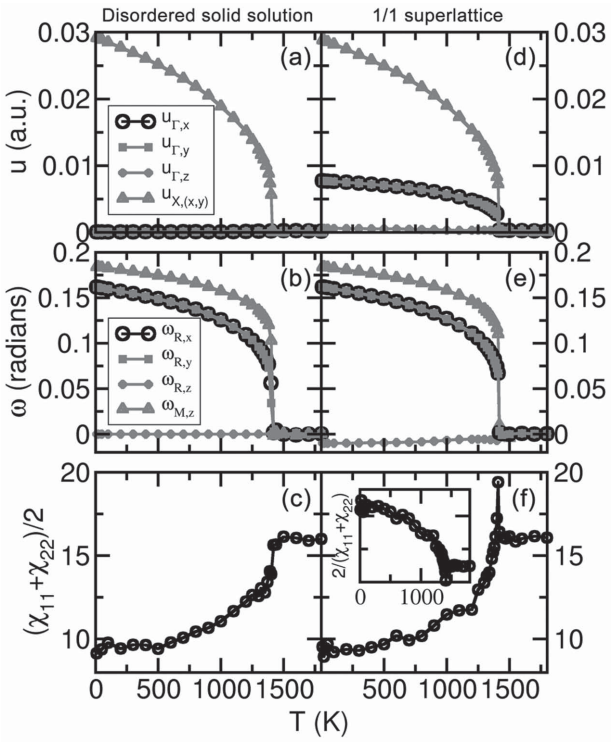

Figure 1. a,d) Temperature dependence of the supercell averages of the local modes (u_Γ and u_x characterizing ferroelectricity and antiferroelectricity, respectively); b,e) antiphase and in-phase oxygen octahedra tilting vectors (ω_R and ω_M); c,f) and the in-plane dielectric susceptibility of a–c) $Bi_{0.5}Nd_{0.5}FeO_3$ disordered solid solution and d–f) 1/1 superlattice. The inset of (f) shows the inverse of the dielectric susceptibility of the 1/1 superlattice.

octahedral tiltings, respectively, occur, while their magnitudes are the rotation amplitudes; and (iii) the average in-plane dielectric susceptibility element, $\chi = (\chi_{11} + \chi_{22})/2$, where the indices "1" and "2" correspond to the pseudo-cubic [100] and [010] directions, respectively. Similar data are displayed in Figure 1d–f, but for the superlattice.

Figure 1a–c indicates that the calculations correctly predict the ground state of disordered $(Bi_{0.5}Nd_{0.5})FeO_3$ solid solutions,[31–33] i.e., a nonpolar orthorhombic *Pnma* state that is characterized by an *X*-type AFE vector lying along the pseudocubic [110] direction, antiphase tilting about this [110] direction and in-phase tilting about the perpendicular, pseudocubic [001] direction. These figures also show that such a *Pnma* state transforms into a cubic phase in which all antiferroelectric displacements and oxygen octahedral tiltings vanish, via a first-order transition (as especially evidenced by the significant jump in ω_M) at about 1420 K.

Let us now pay attention to the properties of the ordered system depicted in Figure 1d–f. One most noticeable difference between the SL and the disordered solid solution appears in the ordered phase, as the former possesses a spontaneous electrical polarization lying along the pseudocubic [110] direction, evidenced by the nonzero $u_{\Gamma,x} = u_{\Gamma,y}$ Cartesian components. Such polarization makes the ground state transform from a nonpolar *Pnma* space group in the disordered material to a polar $Pmc2_1$ space group in the superlattice. This polarization is the essence

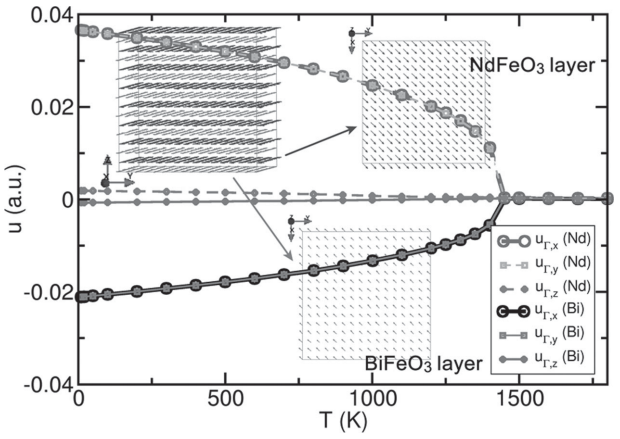

Figure 2. Temperature dependence of the layer-resolved supercell averages of the local modes (u_Γ characterizing the local ferroelectricity) for the BFO and NFO layers of the $(BiFeO_3)_1/(NdFeO_3)_1$ superlattice. The insets illustrate the superlattice structure with light gray and dark gray arrows indicating the local dipoles of Bi- and Nd-centered sites, respectively.

of the hybrid improper ferroelectricity[5,6,11] and, on a microscopic level, arises from the fact that the (larger) motions of Nd atoms parallel to the [110] direction are not fully compensated by the (smaller) displacements of the Bi atoms in the opposite direction—as revealed by **Figure 2**, which displays the layer-resolved temperature dependences of the averaged local modes of BFO and NFO layers. As shown in Figure 1d, such non-compensation generates values of $u_{\Gamma,x} = u_{\Gamma,y} = 0.0077$ in lattice units at 10 K, according to our Monte Carlo (MC) simulations. Such values are numerically found to correspond to a spontaneous electrical polarization of 7.43 μC cm^{-2} along the [110] direction, which agrees rather well with the net polarization of 6.91 μC cm^{-2} obtained when performing a direct density functional theory (DFT) investigation of the SL ground state at 0 K. Note that these DFT computations also confirm that the magnitude of the Nd ions' displacement along [110] is larger than that of the Bi ions in the opposite direction within the considered 1/1 BFO/NFO superlattice, which further attests the accuracy of our effective Hamiltonian method. (In the SL we also obtain a very small nonzero $u_{\Gamma,z}$ (Figures 1d and 2), and accordingly a small nonzero component of the antiphase tilting (Figure 1e). These out-of-plane distortions are at least one order of magnitude smaller than the corresponding in-plane components, as also consistent with the DFT calculations we conducted. They will therefore be neglected in the discussion below.) Figure 2 also indicates that this hierarchy between the magnitude of the Nd and Bi ions' displacements remains valid when heating the superlattice up to $T_C = 1420$ K, and accompanies the resulting decrease of the polarization with temperature as shown in Figure 1d. At that latter critical temperature, Figure 1d,e reveals that the polarization, along with the AFE vector and the antiphase and in-phase tiltings, suddenly disappears via a first-order transition to a nonpolar (*P4/mmm*) state. Such simultaneous disappearance is a consequence of the fact that, at a macroscopic level, the spontaneous polarization in HIF materials originates from a trilinear energy coupling between this polarization and these two different types of oxygen octahedral tiltings.[5,6,11] It is also important to realize that the polarization shown in Figure 1d is numerically found to be a square-root function of the temperature just below T_C. We will come back to that point later.

It is also interesting to examine how the dielectric response—resulting from this new form of ferroelectricity and associated trilinear coupling—behaves as a function of temperature. In particular, does this dielectric response (i) exhibit Curie–Weiss behavior above and below T_C as in proper ferroelectrics; or (ii) is it constant with temperature above and below T_C, with a discontinuity occurring at the transition point as in second-order improper ferroelectrics;[13] or (iii) roughly follows the Curie–Weiss law below T_C, while suddenly decreasing at T_C, and then becoming a constant above T_C, as in triggered-type ferroelectrics;[14,15] or (iv) inversely depends on the square-root of temperature below T_C, and drops to a constant above T_C, as in first-order improper ferroelectrics?[13] Figure 1f, which displays the behavior of the calculated dielectric susceptibility, χ, of the superlattice as a function of temperature, provides an answer to this question. As a matter of fact, one can see that χ is basically a constant above T_C, unlike in case (i). Moreover, χ varies with temperature below T_C, which also rules out case (ii). Furthermore, the dielectric response shown in Figure 1f possesses a discontinuity at the transition temperature, which seems to be similar to case (iii), but the temperature dependence deviates apparently from the Curie–Weiss law (inset of Figure 1f). Interestingly, it rather shows a close resemblance to case (iv) close to the phase transition, which will be inspected quantitatively in next section. We also notice that the maximum magnitude of the dielectric susceptibility in HIF is much less than that reported for the nonproper PTO/STO SL (≈600),[34] and a comparison between χ shown in Figure 1c for the disordered solid solution and in Figure 1f for the superlattice reveals that these two dielectric responses are essentially identical to each other except at temperatures a few tens of Kelvin below T_C (for which the dielectric response of the SL varies strongly and displays a peak). Such surprising result therefore demonstrates that HIF and its associated trilinear coupling have basically no effect on the dielectric response, except when being very close to the transition point.

2.2. Landau Model and Hybrid Improper Ferroelectricity

In order to gain a deeper understanding of the results provided by our numerical microscopic approach, we decided to develop a phenomenological Landau theory for which the free energy of our SLs is of the following form

$$\begin{aligned} F = {} & A_1(T - T_0)\omega^2 + A_2\omega^4 + A_3\omega^6 \\ & + C_1 X\omega_R\omega_M + C_2 X^2 + C_3 P\omega_R\omega_M + C_4 P^2 \\ & + C_5\left(P^2\omega_R^2 + P^2\omega_M^2\right) - PE \end{aligned} \quad (1)$$

where ω is defined as $\left(\frac{\omega_R}{\sqrt{2}}, \frac{\omega_R}{\sqrt{2}}, \omega_M\right)$ in the Cartesian basis, with ω_R and ω_M being the macroscopic (averaged) magnitudes of the antiphase and in-phase oxygen octahedra tiltings, respectively. Note that using a single order parameter for the tilting in the Landau model is based on our numerical observation that the two tiltings (ω_R and ω_M) change coherently with

temperature. X and P are the macroscopic (averaged) magnitudes of the AFE vector corresponding to the X-point of the first Brillouin zone and the electrical polarization, respectively. E is the external electric field. Finally, T_0 is the critical temperature associated with ω, and the A and C coefficients are all temperature independent. Equation (1) implicitly assumes that, as consistent with first-principles calculations,[9] the *primary* order parameters are the oxygen octahedral tiltings (ω or equivalently ω_R and ω_M), whose temperature dependences are explicitly given by the prefactor of the quadratic term, i.e., $A_1 (T - T_0)$. Equation (1) includes *even* terms up to the sixth order in these tiltings to account for the first-order character of the transition depicted in Figure 1. Only two terms involving the AFE vector are considered in Equation (1): the quadratic term C_2X^2 and the trilinear term $C_1X\omega_R\omega_M$ that has been derived in refs. [4,10] to explain the universal coupling between AFE and AFD motions. As demonstrated in refs.[8,9], such trilinear coupling can be rather strong, which explains why we neglect biquadratic expressions of the form $X^2\omega_R^2$ and $X^2\omega_M^2$ in Equation (1). On the contrary, the polarization appears via *three* different types of energy terms in Equation (1): the harmonic energy C_4P^2, the trilinear energy $C_3P\omega_R\omega_M$ (which, as shown in ref.[11], can be rather weak as compared with $C_1X\omega_R\omega_M$) and the biquadratic interactions of the form $C_5\left(P^2\omega_R^2 + P^2\omega_M^2\right)$. Note that the strength of the $P^2\omega_R^2$ and $P^2\omega_M^2$ interactions are supposed to be characterized by the same C_5 coefficient because these interactions can be assumed to have the same atomistic origin.[35]

Equation (1) naturally implies that both X and P are secondary order parameters that can only appear via their trilinear coupling with antiphase and in-phase octahedra tiltings (assuming that the C_2, C_4, and C_5 coefficients are all positive). Note that in many materials of interest (e.g., Bi-based perovskites) the off-centering of the A-site cations (and, thus, the associated FE and AFE modes) may constitute instabilities of the high-symmetry structure; yet, in the orthorhombic compounds investigated here, we can assume that the structural phase transition occurs at very high temperatures at which these modes are still stable and, thus, their energy can be described by a positive quadratic term.

Minimizing the proposed Landau energy with respect to X leads to

$$X = -\frac{C_1}{2C_2}\omega_R\omega_M \tag{2}$$

In other words, the AFE vector should be directly dependent on the product between antiphase and in-phase tilting angles, with the coefficient of proportionality being independent of temperature. **Figure 3**a reports the behavior of X as a function of $\omega_R\omega_M$ resulting from our MC simulations in the investigated superlattice for all computed temperatures below T_C. A linear dependence is indeed observed, as consistent with the phenomenological Equation (2).

Setting now to zero the first-order derivative of the free energy of Equation (1) with respect to P yields

$$P = \frac{E - C_3\omega_R\omega_M}{2C_4 + 2C_5(\omega_R^2 + \omega_M^2)} \tag{3}$$

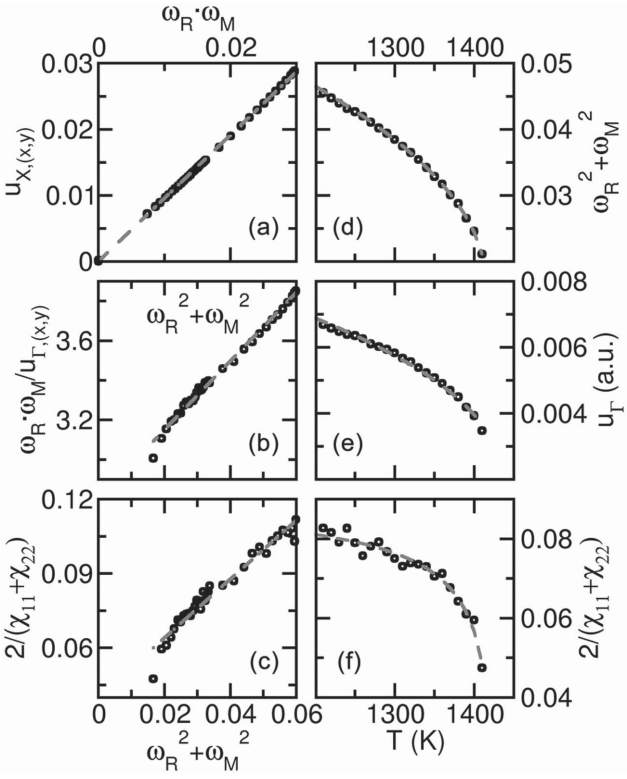

Figure 3. Verification of the applicability of the Landau model (dashed lines) to reproduce and understand the numerical output data of the MC simulations (discrete points) for the $(BiFeO_3)_1/(NdFeO_3)_1$ superlattice. a) u_x (characterizing antiferroelectricity) as a function of $\omega_R\omega_M$, the dashed line is from the linear fitting predicted by Equation (2); b) $\omega_R\omega_M/P$ as a function of $\omega_R^2 + \omega_M^2$, the dashed line is from linear fitting given by Equation (3); c) $2/(\chi_{11} + \chi_{22})$ as a function of $\omega_R^2 + \omega_M^2$, the dashed line is from linear fitting associated with Equation (4); d) $\omega_R^2 + \omega_M^2$ as a function of temperature, the dashed curve is fitted with Equation (6); e) P as a function temperature, the dashed curve is fitted with Equation (7); f) $2/(\chi_{11} + \chi_{22})$ as a function of temperature, the dashed curve is fitted with Equation (5).

This latter equation indicates that the ratio $\omega_R\omega_M/P$ should be directly proportional to $\omega_R^2 + \omega_M^2$ when there is no external electric field ($E = 0$). Except close to the phase transition, and as revealed by Figure 3b, such dependence is indeed confirmed by the results of the MC simulations in the SL.

It is also important to realize that, as consistent with refs. [4,11], the "only" distinction between the SL and disordered solution within the phenomenological model concerns the C_3 coefficient of the trilinear coupling: this coefficient is finite for the superlattice while it vanishes for the disordered solid solution. As a result, the existence of the C_3 parameter in Equation (3) provides a successful explanation of why the spontaneous polarization can only appear in the superlattice (when $E = 0$).

Our phenomenological model also allows the derivation of the dielectric susceptibility via $\chi = \partial P/\partial E$ with the polarization being given by Equation (3). The resulting inverse of the dielectric susceptibility is

$$\frac{1}{\chi} = 2C_4 + 2C_5(\omega_R^2 + \omega_M^2) \tag{4}$$

when assuming that the tiltings do not depend on the electric field.

Equation (4) implies that (i) the dielectric response should be a constant for temperature above T_C since the antiphase and in-phase tiltings vanish there; (ii) the inverse of the dielectric susceptibility should be linearly dependent on $\omega_R^2+\omega_M^2$ for temperatures below T_C; and (iii) the dielectric response should "jump up" when heating the system and then crossing the transition temperature (i.e., when ω_R and ω_M suddenly disappear via a first-order transition) because the C_5 coefficient is positive, as consistent with the typical biquadratic repulsion between polarization and tilting of oxygen octahedra (see, e.g., ref. [35], and references therein). Our MC simulations confirm that point (i) is satisfied in both the SL and disordered alloy (see Figure 1c,f). Point (ii) is also found to be obeyed in these two systems, except at temperatures slightly below T_C in the SL (see Figure 3c). Moreover, point (iii) is only followed in the disordered alloy, i.e., it is not valid in the SL (see Figure 1c,f). As shown in Figures S1 and S2 (Supporting Information), the difference in dielectric response in the vicinity below T_C between the SL and disordered solid solution comes from the fact that the assumption (that led to the derivation of Equation (4)) that the oxygen octahedral tilting are independent of electric field does not hold in the SL close to the phase transition. Further derivations detailed in the Supporting Information (and going beyond the aforementioned assumption) reveal that the dielectric response of the SL should, in fact, obey the following equation rather than Equation (4), close to the phase transition

$$\frac{1}{\chi_{SL}}=2C_4-\frac{C_3'^2}{2\sqrt{A_2^2-3A_1A_3(T-T_0)}} \quad (5)$$

where C_3' is proportional to C_3 (see definition in the Supporting Information). Interestingly, this latter dependence of the dielectric response in the SL is indeed confirmed by our MC simulations (c.f. Figure 3f) and also explains why the dielectric response is strongly enhanced just below T_C in the SL while not in the disordered solution since Equation (5) involves the C_3 coefficient (which is nonzero only in the SL).

The Supporting Information further shows that, just below T_C, the temperature dependence of AFD tiltings and polarization can be derived to be

$$\omega^2=\omega_R^2+\omega_M^2=-\frac{A_2}{3A_3}+\frac{\sqrt{A_2^2-3A_1A_3(T-T_0)}}{3A_3} \quad (6)$$

$$P=\frac{A_2C_3'}{6A_3C_4}-\frac{C_3'\sqrt{A_2^2-3A_1A_3(T-T_0)}}{6A_3C_4} \quad (7)$$

As demonstrated by Figure 3d,e, good fittings of the MC results in a temperature range extending about 200 K below the phase transition can indeed be obtained by Equations (6) and (7), respectively, with T_0 being found to be 1370 K. Note that the fact that T_0 is lower than T_C is consistent with the first-order nature of the transition.

Interestingly, the temperature dependences of the polarization and dielectric response given by Equations (7) and (5), respectively, are exactly those expected in first-order improper ferroelectrics.[13] In particular, our findings suggest that the studied superlattice should be described as a regular (first-order) improper ferroelectric rather than as a "hybrid" one.[7] This conclusion relies on the fact that the free energy (close to the phase transition) given in Equation (1) of the Supporting Information is very similar to the one introduced in the "classical" paper of improper ferroelectrics,[13] with an identical temperature dependence of the two primary order parameters and the same trilinear coupling between these two order parameters and the polarization.

2.3. Switching Mechanism

Let us now determine if the HIF polarization can be switched by an electric field.

First, we use the effective Hamiltonian described above and apply an electric field along the $[\bar{1}\bar{1}0]$ direction (i.e., opposite to the initial net polarization), continuously increasing its magnitude. Our numerical results (not shown here) show that the electric dipoles in the BFO and NFO layers are relatively unresponsive to this field, and continue to be oriented along the $[\bar{1}\bar{1}0]$ and [110] directions, respectively (as shown in Figure 2). At the same time, the Bi-related dipoles become larger than those associated to the Nd off-centering. As a result, the net polarization reverts its sign while the AFE vector does not. Moreover, during this process, the oxygen octahedral tiltings are found to be almost unchanged, and the system returns to its initial state when the electric field is removed. Hence, by applying an electric field in this particular way we succeeded in changing the sign of the polarization, but the system did not reach an equilibrium state; hence, the switching did not actually occur.

This impossibility to go from one equilibrium state to an equivalent equilibrium state of the energy, by applying an electric field opposed to the initial polarization, suggests that a large energy barrier exists between these two minima when following this path.

One may thus wonder whether there are alternative polarization switching paths that can allow the system to jump between two equilibrium states with the same energy, a process that—because of the trilinear coupling $C_3P\omega_R\omega_M$—will necessarily involve a reversal of one of the rotational distortions. In particular, we want to check if the mechanism identified in ref.[9] and involving the rotation of the polarization is feasible. For that, we consider a five-state process. First we apply an electric field, at 10 K, along the $[\bar{1}10]$ direction (which is thus perpendicular to the polarization of the initial state), and progressively increase its magnitude (up to 4.0×10^9 V m^{-1}). **Figure 4**a shows that the polarization rotates from the [110] direction toward the $[\bar{1}10]$ direction, and grows in magnitude, when this field continuously increases from 0 to 3.4×10^9 V m^{-1} (note that the mimicked electric fields in the MC simulations are typically larger than the corresponding experimental fields by a factor of about 25[36] and that, nevertheless, a field of 10^9 V m^{-1} has recently been applied to BFO films in some measurements [37]; hence, our simulations correspond to an experimentally achievable situation). Then, at this critical field, a first-order

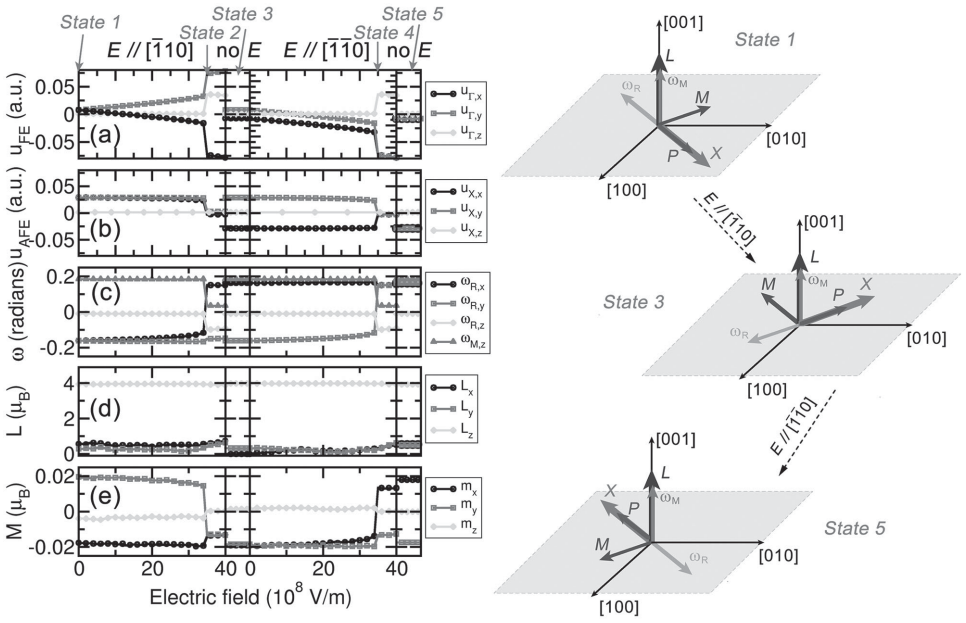

Figure 4. The five-state switching mechanism for $(BiFeO_3)_1/(NdFeO_3)_1$ superlattice. a,b) The local modes (upper panel: u_Γ; lower panel: u_x characterizing ferroelectricity and antiferroelectricity, respectively); c) oxygen octahedra tilting vectors (ω_R and ω_M characterizing antiphase and in-phase tiltings, respectively); d) the AFM vector; and e) the weak FM vector under a sequence of applied electric fields, i.e., 1) an increasing field along the $[\bar{1}10]$ direction (perpendicular to the initial polarization); 2) field removed; 3) an increasing field along the $[\bar{1}\bar{1}0]$ direction (antiparallel to the initial polarization); 4) field removed. The insets show schematics of the five-state switching mechanism.

transition occurs, which results in a dramatic enhancement of the in-plane polarization along the direction of the applied electric field, along with the appearance of the *z*-component of the polarization (state 2, see Figure 4a) and the disappearance of the antipolar mode (cf. Figure 4b). At this critical field, the antiphase AFD vector also changes abruptly, with its in-plane component switching from the $[\bar{1}\bar{1}0]$ to $[1\bar{1}0]$ direction—as shown in Figure 4c—since this in-plane component wants to be parallel or antiparallel to the in-plane component of the polarization (i.e., it is energetically costly for a polarization and antiphase AFD vector to be along orthogonal directions.[15]) A small out-of-plane component also appears for ω_R (due to the fact that the polarization has also a *z*-component) and the in-phase tilting ω_M drops to a very small value. Then the large field is removed from state 2, which yields state 3, with a polarization, AFE vector and antiphase and in-phase tiltings that have precisely the same magnitude as their initial values (i.e., state 1), but with the polarization and AFE vector having all rotated from [110] to $[\bar{1}10]$ while ω_R has switched from $[\bar{1}\bar{1}0]$ to $[1\bar{1}0]$ and ω_M remains oriented along the [001] axis. Such evolutions are consistent with the action of the $C_3P\omega_R\omega_M$ and $C_1X\omega_R\omega_M$ trilinear couplings indicated in Equation (1). Starting from state 3, an electric field along the $[\bar{1}\bar{1}0]$ direction (which is thus now opposed to the initial polarization) is then applied, and increased up to 4.0×10^9 V m^{-1}. Figure 4a–c shows that the structural response as a function of this field is analogous to the one obtained when going from state 1 to states 2 and 3. For instance, there is a critical field of 3.4×10^9 V m^{-1}, at which the FE, AFE vectors, and AFD motions all change abruptly, yielding state 4. With the removal of the large electric field of 4.0×10^9 V m^{-1} that is applied along the $[\bar{1}\bar{1}0]$ direction, we reach the final state 5 with the polarization and ω_R being exactly equal in magnitude but opposed in direction to those in the initial state (that is, corresponding to state 1) while the in-phase AFD vectors of the initial and final states are identical to each other—as consistent with the $C_3P\omega_R\omega_M$ trilinear coupling. Interestingly, the AFE vector has also reversed its direction from [110] to $[\bar{1}10]$ between state 1 and state 5, as dictated by the other $C_1X\omega_R\omega_M$ trilinear coupling. Such reversal also implies that the (smaller) electric dipoles of the BFO layers now lie along the [110] direction while those (larger) coming from the NFO layers are now oriented along the $[\bar{1}\bar{1}0]$ direction. According to our Landau model described by Equation (1), the simultaneous switchings of *P*, *X*, and ω_R—while ω_M remains unchanged—yield a final state that has the same free energy as the initial state.

Let us now see if these switchings have some effect on magnetism. As shown in Figure 4d,e, the initial state has a G-type AFM vector ***L*** lying along the [001] direction with a magnitude of about $4\mu_B$, while the weak ferromagnetic moment ***M*** is along the $[\bar{1}10]$ direction with a magnitude of $0.027\mu_B$. This is the so-called Γ_2 magnetic state, which is known to occur in orthoferrites.[38–40] Interestingly, during the whole aforementioned five-state process, ***L*** remains unchanged while ***M*** undergoes striking changes not only in magnitude but also in direction. For instance, in state 5, ***M*** lies along the $[1\bar{1}0]$ direction that is precisely opposed to its initial direction. In other words, the described five-state switching process has resulted in the full reversal of the magnetization. This is a remarkable magneto-electric effect clearly reminiscent of the recent finding that the weak ferromagnetism in the *R*3*c* phase of pure BFO can be switched by an applied electric field via a two-step polarization-rotation path.[41]

Interestingly, our presently discovered magneto-electric effect can be easily understood when recalling a recent work

showing that the magnetic vectors, $\boldsymbol{L}$ and $\boldsymbol{M}$, couple to the antiphase tilting vector ω_R through a universal energetic term of the form $K\boldsymbol{\omega}_R \cdot (\mathbf{L}\times\mathbf{M})$, where K characterizes the strength of this coupling.[42] Since $\boldsymbol{L}$ remains unchanged during the five-state process, this universal coupling term implies that a change in magnitude/direction of ω_R should automatically be accompanied by a concomitant change in magnitude/direction of $\boldsymbol{M}$ (provided that ω_R and $\boldsymbol{L}$ are not parallel to each other). Figure 4c,e confirms that this is indeed the case. As schematized in the right panel of Figure 4, this five-state process therefore allows a deterministic electric-field-induced reversal of many quantities (namely, polarization, AFE vector, antiphase tilting, and magnetization) thanks to the existence and combination[42] of the three trilinear energy couplings $C_3P\omega_R\omega_M$, $C_1X\omega_R\omega_M$, and $K\boldsymbol{\omega}_R \cdot (\mathbf{L}\times\mathbf{M})$.[43]

3. Conclusions

In summary, an effective Hamiltonian numerical scheme has been used to study finite-temperature properties of a prototype of HIF, i.e., the short period $(BiFeO_3)_1/(NdFeO_3)_1$ superlattice. We have discussed in detail the temperature dependence of the polarization, oxygen octahedra tiltings, and dielectric susceptibility—always comparing our superlattice results with those obtained for a disordered $Bi_{0.5}Nd_{0.5}FeO_3$ alloy—and described the main effects with a proposed Landau-type free-energy formalism. In particular, we found and explained that the polarization and dielectric response behave, near the phase transition, in the same way as in first-order improper ferroelectrics. Another important result is the successful demonstration of a five-state switching mechanism that allows to electrically control not only the spontaneous polarization and the magnetization, but also the AFE vector and antiphase tilting, thanks to three different trilinear energy couplings. We hope that our predictions will all be experimentally checked soon and will open the door for the design of novel devices.

4. Experimental Section

MC Simulation and Effective Hamiltonian: We study the finite-temperature properties of BNFO with MC simulations, in which the total energy is calculated using an effective Hamiltonian approach. Both ordered (1/1 superlattice) and disordered (solid solutions) $Bi_{0.5}Nd_{0.5}FeO_3$ are simulated with a 16 × 16 × 16 supercell (thus containing 20 480 atoms). The 1/1 superlattice is constructed with alternating BFO/NFO layers along [001] direction. In the 50% alloy structure, Nd atoms are randomly distributed. Most calculations adopted 20 000 MC sweeps for equilibration and an additional 20 000 MC sweeps for calculation of the statistical thermal averages, whereas up to 200 000 MC sweeps were used for equilibration in some critical points (where phase transition occurs) to ensure converged results. Our effective Hamiltonian (H_{eff}) approach for BNFO systems include the following degrees of freedom: (1) the local mode $\{u_i\}$ centered on the A site i (i.e., on Bi or Nd ions), which are directly related to the local electric dipole centered at the cell i[44,45]; (2) the homogeneous $\{\eta_H\}$ and inhomogeneous $\{\eta_I\}$ strain tensors[44,45]; (3) the pseudovector $\{\omega_i\}$ that characterizes the oxygen octahedral tilting about the Fe site i[35]; and (4) the magnetic moment $\{m_i\}$ of the Fe ion located at the site i. σ_j being equal to 0 or +1 is also introduced to account for the presence of a Bi or Nd ion at the A-lattice site j, respectively. We also define a local quantity $\eta_{loc}(i)$ centered on the Fe-site i as $\eta_{loc}(i)=\frac{\delta R_{ionic}}{8}\sum_j \sigma_j$, where the sum over j runs over the eight A nearest neighbors of eight Fe-site i and δR_{ionic} represents the relative difference in ionic radius between Nd and Bi ions. $\eta_{loc}(i)$ is therefore different from zero only if at least one of these eight A sites are occupied by the Nd ions, i.e., it vanishes for pure BFO. The total energy of this H_{eff} has two main terms

$$E_{tot} = E_{BFO}(\{u_i\},\{\eta_H\},\{\eta_I\},\{\omega_i\},\{m_i\}) + E_{alloy}(\{u_i\},\{\omega_i\},\{m_i\},\{\eta_{loc}\}) \quad (8)$$

where E_{BFO} is the effective Hamiltonian of pure BFO[25,46–48] and E_{alloy} characterizes the effect of substituting Bi by Nd ions. Details about this method can be found in ref.[16] and references therein. Nevertheless, it is worth to point out that, as demonstrated in ref.[11], the two trilinear coupling terms existing in the proposed Landau model ($C_3P\omega_R\omega_M$ and $C_1X\omega_R\omega_M$ in Equation (1)) result from the following energy term

$$\Delta E_1 = \sum_i \sum_{l,m,n=0,1} \sum_{\substack{\alpha,\beta=x,y,z \\ \alpha\neq\beta}} K_{1i}(-1)^{(lx+my+nz)_\alpha}\,\omega_{ilmn,\alpha}u_{i,\beta}\omega_{ilmn,\beta} \quad (9)$$

appearing in E_{tot}, where the summation over i runs over all the five-atom unit cells, and x, y, z are chosen to lie along the pseudocubic [100], [010], and [001] directions, respectively. $\omega_{ilmn,\alpha}$ denotes the octahedra tiltings that are within the reach from site i by a lattice vector $a_{lat}(lx+my+nz)$ with l, m, n = 0 or 1. In particular, the net HIF polarization in the 1/1 superlattice arises from the difference in the coefficient K_{1i} for the sites containing Bi versus Nd ions. Note that, for the solid solution, the net polarization is averaged out to be zero due to the random distribution of the Bi and Nd cations. Moreover, the universal coupling between the antiphase tiltings and the magnetism $K\boldsymbol{\omega}_R \cdot (\mathrm{L}\times\mathrm{M})$ is also incorporated in E_{tot} via the following energy term[42]

$$\Delta E = K\sum_{i,j}(\omega_i-\omega_j)\cdot(\mathrm{m}_i-\mathrm{m}_j) \quad (10)$$

where i and j run over all the Fe sites with a cutoff distance up to the first-nearest neighbors. K is a material-dependent coefficient that characterizes this coupling strength. Note that Equation (10) resembles the form of the Dzyaloshiskii–Moriya interaction[29,30] $\boldsymbol{D}'\cdot(\mathrm{m}_i-\mathrm{m}_j)$, such that the $\boldsymbol{D}'$ vector is the difference of octahedral tiltings between site i and site j.

Supporting Information

Supporting Information is available from the Wiley Online Library or from the author.

Acknowledgements

This work was financially supported by the Department of Energy, Office of Basic Energy Sciences, under Contract No. ER-46612 (B.X. and L.B.) and by the NSF Grant No. DMR-1066158 (D.W.). D.W. acknowledges the support from the NSFC Grant No. 51390472 and the 111 Project (B14040). J.I. was financially supported by the Fond National de Recherche Luxembourg through PEARL (Grant No. FNR/P12/4853155/Kreisel) and by MINECO-Spain (Grant No. MAT2013–40581-P). X.M.C. was financially supported by NSFC under Grant No. 51332006. The authors are thankful for discussions with Dr. Y. Yang.

Received: March 19, 2015
Published online: May 12, 2015

[1] W. Eerenstein, N. D. Mathur, J. F. Scott, *Nature* **2006**, *442*, 759.
[2] M. Bibes, A. Barthelemy, *Nat. Mater.* **2008**, *7*, 425.
[3] Y. Tokunaga, N. Furukawa, H. Sakai, Y. Taguchi, T. Arima, Y. Tokura, *Nat. Mater.* **2009**, *8*, 558.
[4] H. J. Zhao, W. Ren, Y. Yang, J. Iñiguez, X. M. Chen, L. Bellaiche, *Nat. Commun.* **2014**, *5*, 4021.
[5] J. M. Rondinelli, C. J. Fennie, *Adv. Mater.* **2012**, *24*, 1961.
[6] A. T. Mulder, N. A. Benedek, J. M. Rondinelli, C. J. Fennie, *Adv. Funct. Mater.* **2013**, *23*, 4810.
[7] N. A. Benedek, C. J. Fennie, *Phys. Rev. Lett.* **2011**, *106*, 107204.
[8] M. Stengel, C. J. Fennie, P. Ghosez, *Phys. Rev. B* **2012**, *86*, 094112.
[9] Z. Zanolli, J. C. Wojdeł, J. Íñiguez, P. Ghosez, *Phys. Rev. B* **2013**, *88*, 060102.
[10] L. Bellaiche, J. Íñiguez, *Phys. Rev. B* **2013**, *88*, 014104.
[11] H. J. Zhao, J. Íñiguez, W. Ren, X. M. Chen, L. Bellaiche, *Phys. Rev. B* **2014**, *89*, 174101.
[12] http://yclept.ucdavis.edu/course/240C/Notes/Landau/Landau-PhaseTrans.pdf (accessed: March 2015).
[13] A. P. Levanyuk, D. G. Sannikov, *Uspekhi Fiz. Nauk* **1974**, *112*, 561.
[14] J. Holakovsk, J. Holakovský, *Phys. Status Solidi* **1973**, *615*, 615.
[15] I. Kornev, L. Bellaiche, *Phys. Rev. B* **2009**, *79*, 1.
[16] B. Xu, D. Wang, J. Íñiguez, L. Bellaiche, *Adv. Funct. Mater.* **2015**, *25*, 552.
[17] A. M. Glazer, *Acta Crystallogr., Sect. B: Struct. Crystallogr. Cryst. Chem.* **1972**, *28*, 3384.
[18] S. Geller, E. A. Wood, *Acta Crystallogr.* **1956**, *9*, 563.
[19] M. Marezio, J. P. Remeika, P. D. Dernier, *Acta Crystallogr., Sect. B* **1970**, *26*, 2008.
[20] O. Diéguez, O. E. González-Vázquez, J. C. Wojdeł, J. Íñiguez, *Phys. Rev. B* **2011**, *83*, 94105.
[21] S. V Kiselev, R. P. Ozerov, G. S. Zhdanov, *Sov. Phys. Dokl.* **1963**, *7*, 742.
[22] W. C. Koehler, E. O. Wollan, M. K. Wilkinson, *Phys. Rev.* **1960**, *118*, 58.
[23] H. Béa, M. Bibes, A. Barthélémy, K. Bouzehouane, E. Jacquet, A. Khodan, J.-P. Contour, S. Fusil, F. Wyczisk, A. Forget, *Appl. Phys. Lett.* **2005**, *87*, 72508.
[24] H. Béa, M. Bibes, S. Petit, J. Kreisel, A. Barthélémy, *Philos. Mag. Lett.* **2007**, *87*, 165.
[25] D. Albrecht, S. Lisenkov, W. Ren, D. Rahmedov, I. A. Kornev, L. Bellaiche, *Phys. Rev. B* **2010**, *81*, 140401.
[26] I. Sosnowska, T. P. Neumaier, E. Steichele, *J. Phys. C: Solid State Phys.* **1982**, *15*, 4835.
[27] D. Treves, *J. Appl. Phys.* **1965**, *36*, 1033.
[28] M. Eibschütz, S. Shtrikman, D. Treves, *Phys. Rev.* **1967**, *156*, 562.
[29] I. Dzyaloshinsky, *J. Phys. Chem. Solids* **1958**, *4*, 241.
[30] T. Moriya, *Phys. Rev. Lett.* **1960**, *4*, 228.
[31] I. Levin, S. Karimi, V. Provenzano, C. L. Dennis, H. Wu, T. P. Comyn, T. J. Stevenson, R. I. Smith, I. M. Reaney, *Phys. Rev. B* **2010**, *81*, 020103.
[32] D. Kan, L. Pálová, V. Anbusathaiah, C. J. Cheng, S. Fujino, V. Nagarajan, K. M. Rabe, I. Takeuchi, *Adv. Funct. Mater.* **2010**, *20*, 1108.
[33] S. Karimi, I. M. Reaney, Y. Han, J. Pokorny, I. Sterianou, *J. Mater. Sci.* **2009**, *44*, 5102.
[34] E. Bousquet, M. Dawber, N. Stucki, C. Lichtensteiger, P. Hermet, S. Gariglio, J.-M. Triscone, P. Ghosez, *Nature* **2008**, *452*, 732.
[35] I. Kornev, L. Bellaiche, P. E. Janolin, B. Dkhil, E. Suard, *Phys. Rev. Lett.* **2006**, *97*, 157601.
[36] C. Daumont, W. Ren, I. C. Infante, S. Lisenkov, J. Allibe, C. Carrétéro, S. Fusil, E. Jacquet, T. Bouvet, F. Bouamrane, S. Prosandeev, G. Geneste, B. Dkhil, L. Bellaiche, a Barthélémy, M. Bibes, *J. Phys. Condens. Matter* **2012**, *24*, 162202.
[37] H. Yamada, V. Garcia, S. Fusil, S. Boyn, M. Marinova, A. Gloter, S. Xavier, J. Grollier, E. Jacquet, C. Carrétéro, *ACS Nano* **2013**, *7*, 5385.
[38] R. White, *J. Appl. Phys.* **1969**, *40*, 1061.
[39] J.-H. Lee, Y. K. Jeong, J. H. Park, M.-A. Oak, H. M. Jang, J. Y. Son, J. F. Scott, *Phys. Rev. Lett.* **2011**, *107*, 117201.
[40] H. J. Zhao, W. Ren, Y. Yang, X. M. Chen, L. Bellaiche, *J. Phys. Condens. Matter* **2013**, *25*, 466002.
[41] J. T. Heron, J. L. Bosse, Q. He, Y. Gao, M. Trassin, L. Ye, J. D. Clarkson, C. Wang, J. Liu, S. Salahuddin, D. C. Ralph, D. G. Schlom, J. Íñiguez, B. D. Huey, R. Ramesh, *Nature* **2014**, *516*, 370.
[42] L. Bellaiche, Z. Gui, I. Kornev, *J. Phys. Condens. Matter* **2012**, *24*, 312201.
[43] Y. Yang, J. Íñiguez, A.-J. Mao, L. Bellaiche, *Phys. Rev. Lett.* **2014**, *112*, 057202.
[44] W. Zhong, D. Vanderbilt, K. Rabe, *Phys. Rev. Lett.* **1994**, *73*, 1816.
[45] W. Zhong, D. Vanderbilt, K. Rabe, *Phys. Rev. B* **1995**, *52*, 6301.
[46] S. Prosandeev, D. Wang, W. Ren, J. Íñiguez, L. Bellaiche, *Adv. Funct. Mater.* **2013**, *23*, 234.
[47] I. Kornev, S. Lisenkov, R. Haumont, B. Dkhil, L. Bellaiche, *Phys. Rev. Lett.* **2007**, *99*, 227602.
[48] S. Lisenkov, I. A. Kornev, L. Bellaiche, *Phys. Rev. B* **2009**, *79*, 12101.